



Probing the critical nucleus size in tetrahydrofuran clathrate hydrate formation using surface-anchored nanoparticles


Received: 11 March 2023

Accepted: 11 December 2023

Published online: 02 January 2024



Han Xue^{1,6}, Linhai Li^{1,6}, Yiqun Wang², Youhua Lu¹, Kai Cui¹, Zhiyuan He¹,
Guoying Bai¹, Jie Liu^{1,3}✉, Xin Zhou^{2,4}✉ & Jianjun Wang^{1,3,5}✉



The formation of THF clathrate crystal from solution is determined by the consecutive optical microscopic observation.

¹Beijing National Laboratory for Molecular Science, Key Laboratory of Green Printing, Institute of Chemistry, Chinese Academy of Sciences, Beijing 100190, China. ²School of Physical Sciences, University of Chinese Academy of Sciences, Beijing 100049, China. ³School of Chemical Sciences, University of Chinese Academy of Sciences, Beijing 100049, China. ⁴Wenzhou Institute, University of Chinese Academy of Sciences, Wenzhou 325001, China. ⁵Technical Institute of Physics and Chemistry, Chinese Academy of Sciences, Beijing 100190, China. ⁶These authors contributed equally: Han Xue, Linhai Li.

✉ e-mail: liujie123@iccas.ac.cn; xzhou@ucas.ac.cn; wangjianjun@mail.ipc.ac.cn

A reaction kinetic mechanism for methane hydrate formation in liquid water

Knut Lekvam and Peter Ruoff

Cite this: *J. Am. Chem. Soc.* 1993, 115, 19, 8565–8569

Publication Date: September 1, 1993

<https://doi.org/10.1021/ja00072a007>

© American Chemical Society

[Request reuse permissions](#) [Subscribed](#)

Article Views

784

Altmetric

-

Citations

49

[LEARN ABOUT THESE METRICS](#)

[nature](#) > [articles](#) > article

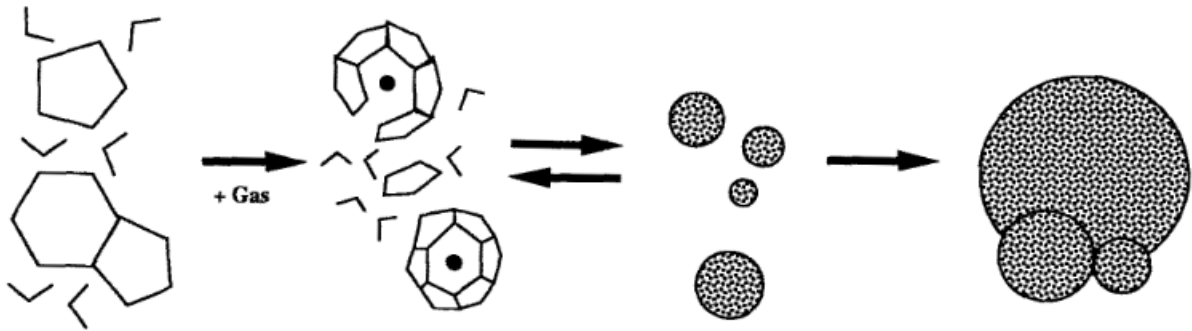
Article | Published: 18 December 2019

Probing the critical nucleus size for ice formation with graphene oxide nanosheets

[Guoying Bai](#), [Dong Gao](#), [Zhang Liu](#), [Xin Zhou](#) & [Jianjun Wang](#)

Nature 576, 437–441 (2019) | [Cite this article](#)

38k Accesses | 268 Citations | 57 Altmetric | [Metrics](#)



A. Initial Condition

Pressure and temperature in hydrate forming region, but no gas molecules dissolved in water

B. Labile Clusters

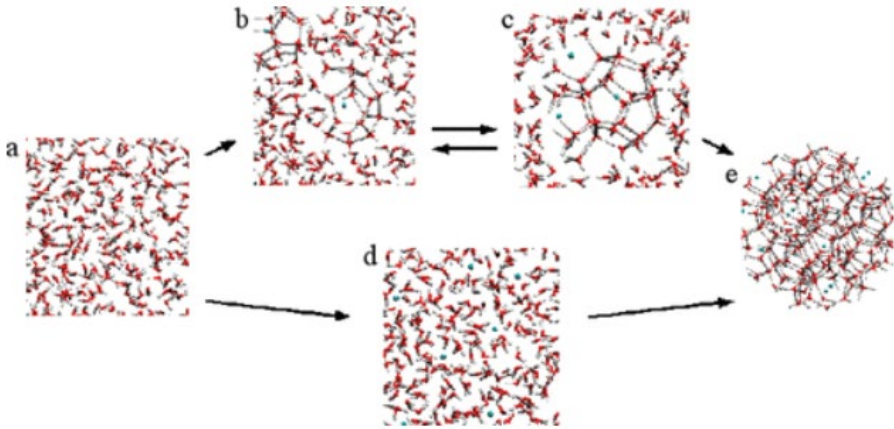
Upon dissolution of gas in water, labile clusters form immediately.

C. Agglomeration

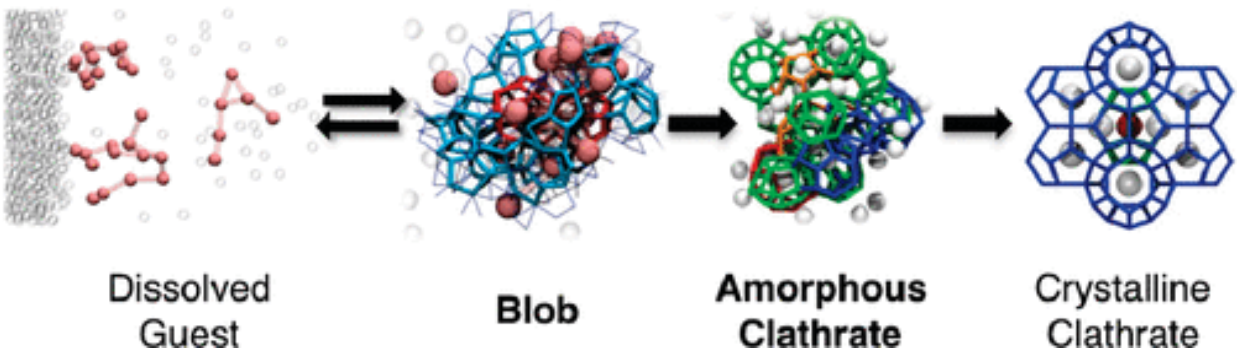
Labile clusters agglomerate by sharing faces, thus increasing disorder.

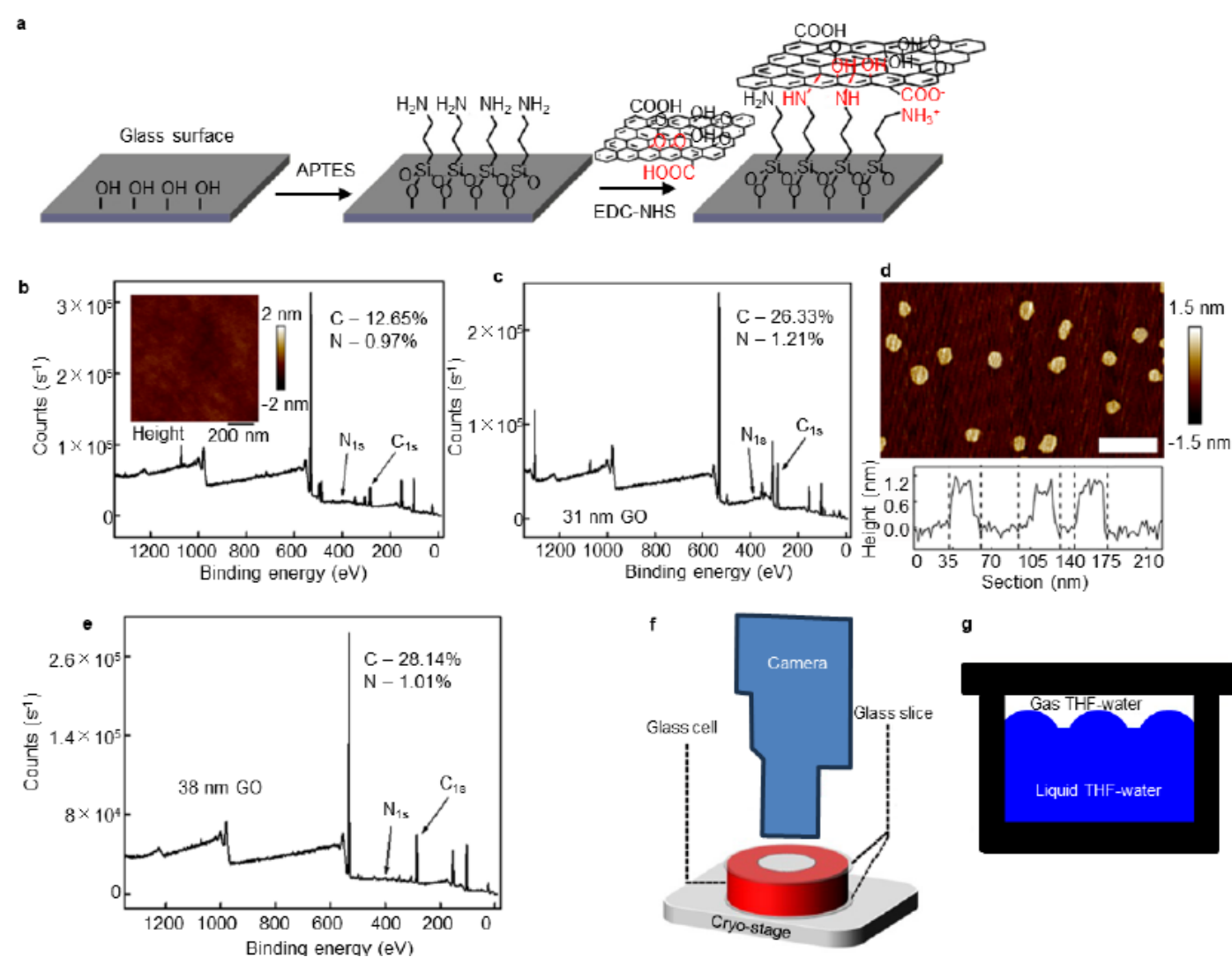
D. Primary Nucleation and Growth

When the size of cluster agglomerates reaches a critical value, growth begins.



Comparison of the cluster nucleation theory (a-b-c-e) and the local structuring hypothesis (a-d-e). (a) Water without dissolved gas molecules (initial condition). (b) Cluster form immediately after dissolution of gas molecules. (c) Cluster prestages agglomerate by sharing faces. These agglomerated clusters may be unstable (step back to b is possible). (d) No cluster formation after dissolution of gas molecules. (e) Hydrate nucleation.





Supplementary Figure 1. Illustration of surface modification and setup of optical observation. **a** Proposed schematic illustration for grafting GOs on the glass substrate. **b** The elemental analysis from XPS spectrum of modified glass substrates with APTES, in which the appearance of N element indicating the APTES grafted. The inset shows the AFM characterizations of the prepared surfaces without GOs. **c** shows the chemical compositions of the glass substrate surfaces anchored with GOs of 31 nm size. **d** shows the AFM imaging of 31 nm GOs and the corresponding height profiles along the blue marked lines. Scale bar, 100 nm. **e** shows the chemical compositions of the glass substrate surfaces anchored with GOs of 38 nm size. From the XPS data, the coverage of anchored GOs can be calculated, in which the GO graft density can be adjusted through changing the reaction time. **f** The sketch of the THF/water sample cell, in which the contact area between the liquid sample and the solid surface can be well quantified through modulating the cell diameter. The clathrate nucleation was monitored through optical microscopy coupled with a high-speed CMOS camera. **g** The side view of experimental glass cell and illustration of gas THF-water between lid and liquid surface.

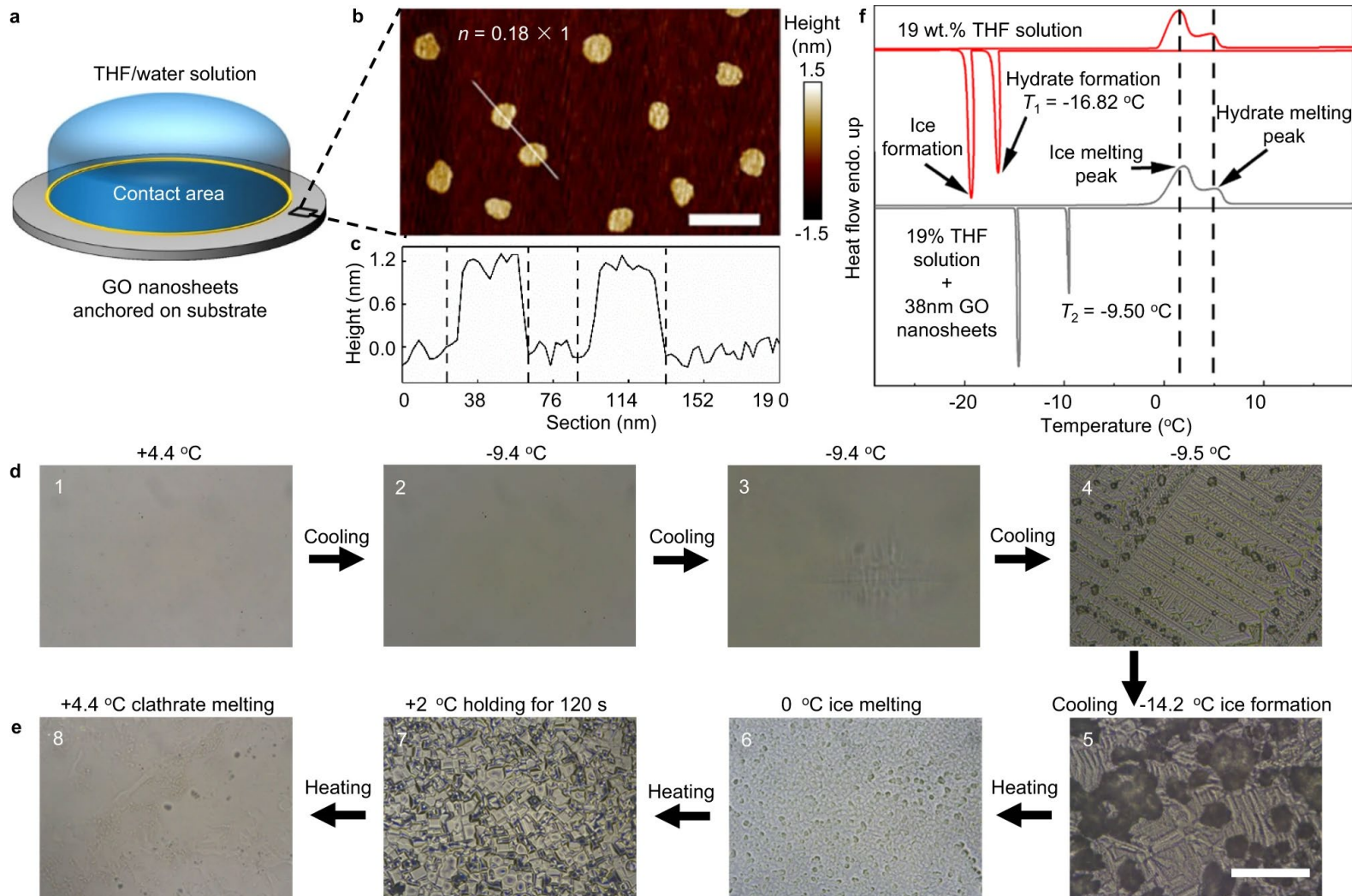
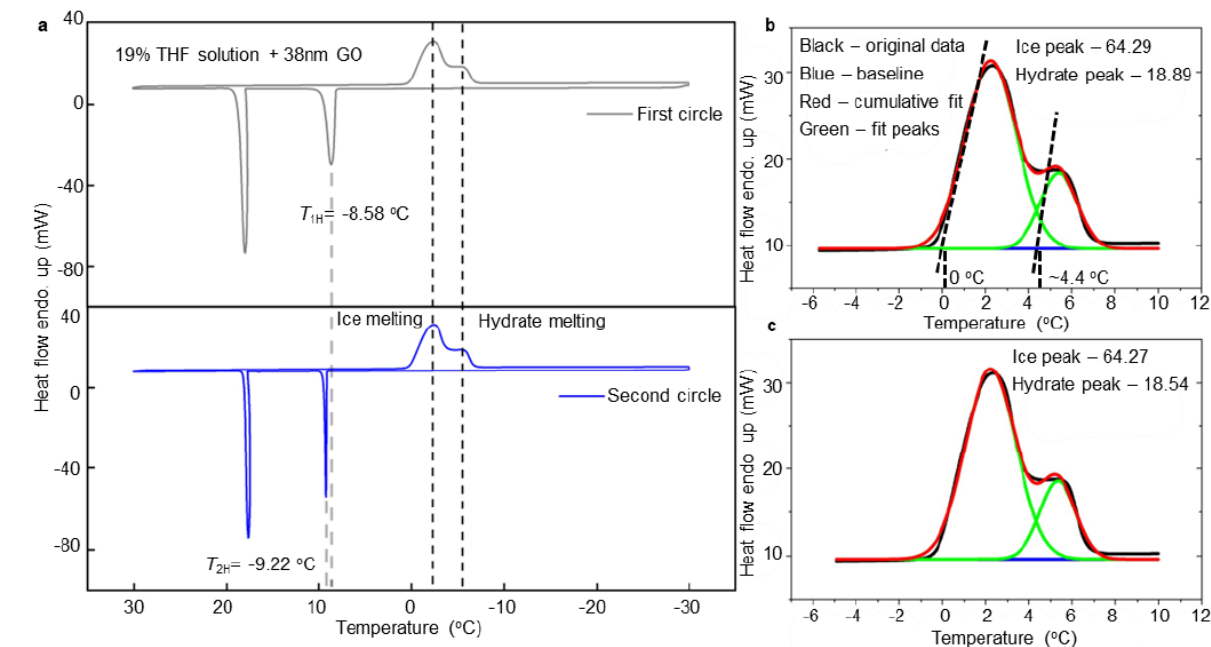
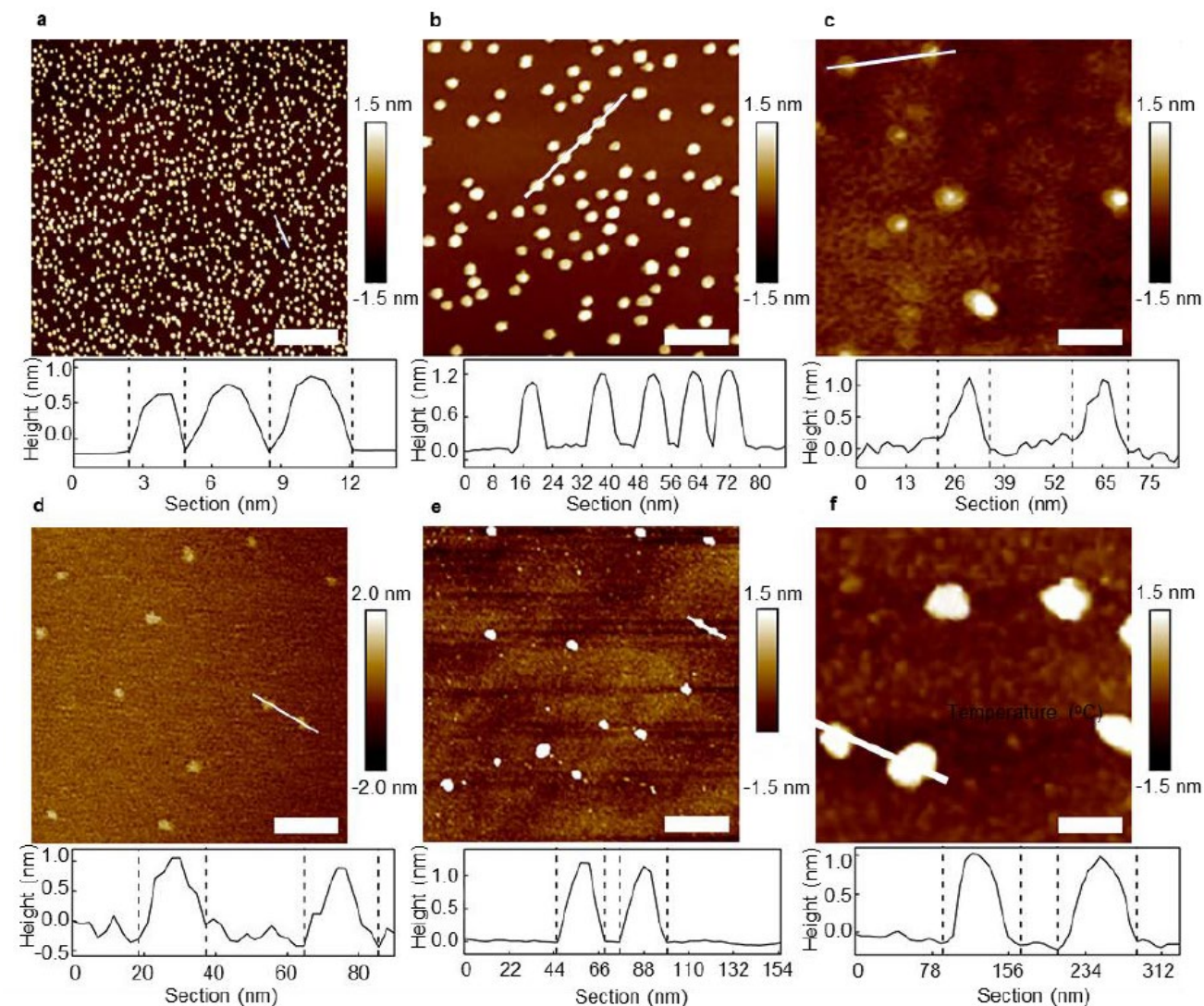


Fig. 1 | The freezing behaviors of THF solution on the GOs anchored glass substrates. **a** Schematic depiction of the THF/water solution deposited on the substrate anchored with GO nanosheets. The blue volume represents the drop of THF solution and the contact area between liquid drop and solid substrate is marked in the yellow circle. **b** shows the AFM images of 38 nm GOs (average lateral size) anchored on the substrate with the scaled coverage $n = 0.18 \times 1$ (relative GO graft density times scaled contact area). Scale bar, 100 nm. **c** shows the corresponding height profiles through the cross-section along the marked lines.

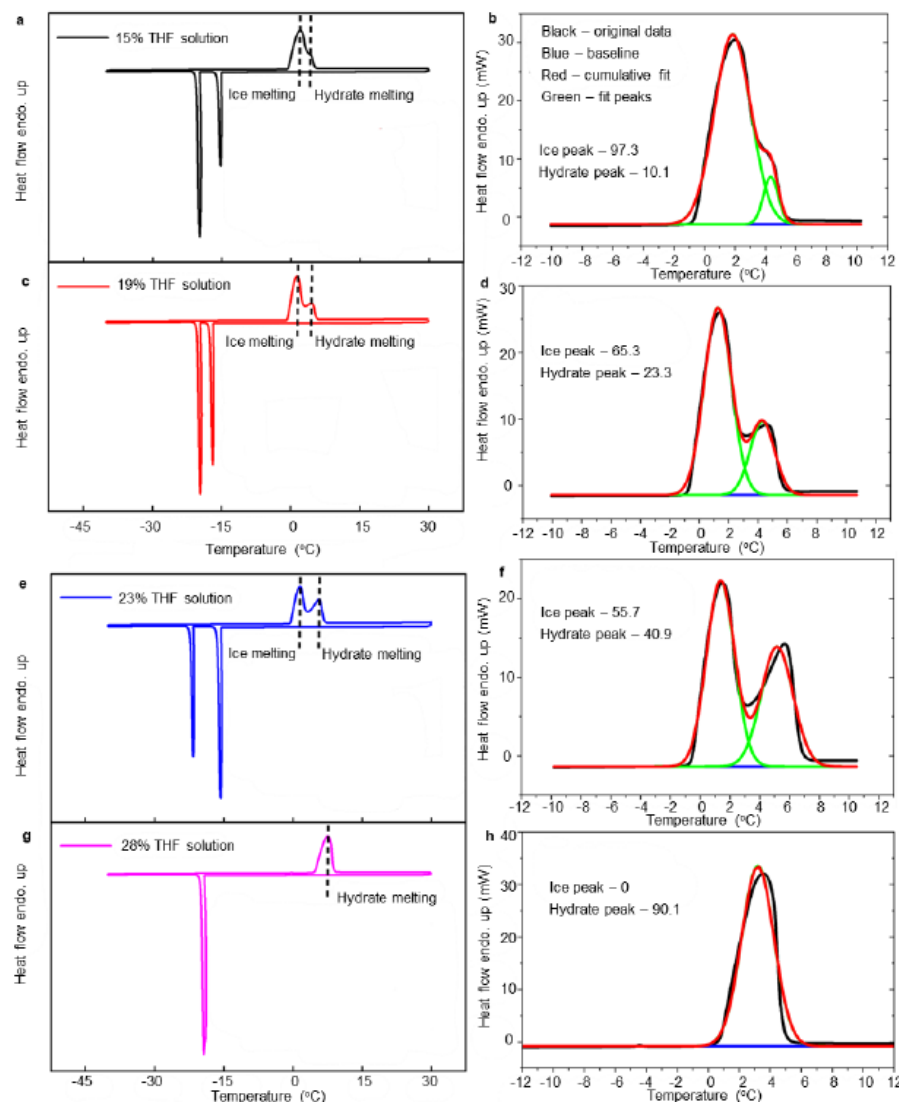
d, e Optical microscopy observation of the formation of THF clathrate (needle-like crystals, step 3) and ice (black and block-like substance, step 5) on the GO anchored surface under microscope in cooling (**d**) then heating (**e**) stages. Cooling rate, 1°C min^{-1} . Sample volume, $3.5\ \mu\text{L}$; the scaled contact area of solution drop, $S = 1$ in the unit $S_0 = 0.25\ \text{mm}^2$; scale bar, $100\ \mu\text{m}$. **f** Thermal analysis of the formation and melting of THF clathrate hydrates and ice on the glass substrate surface without (red line) and with (gray line) the anchored 38 nm GO nanosheets by DSC.



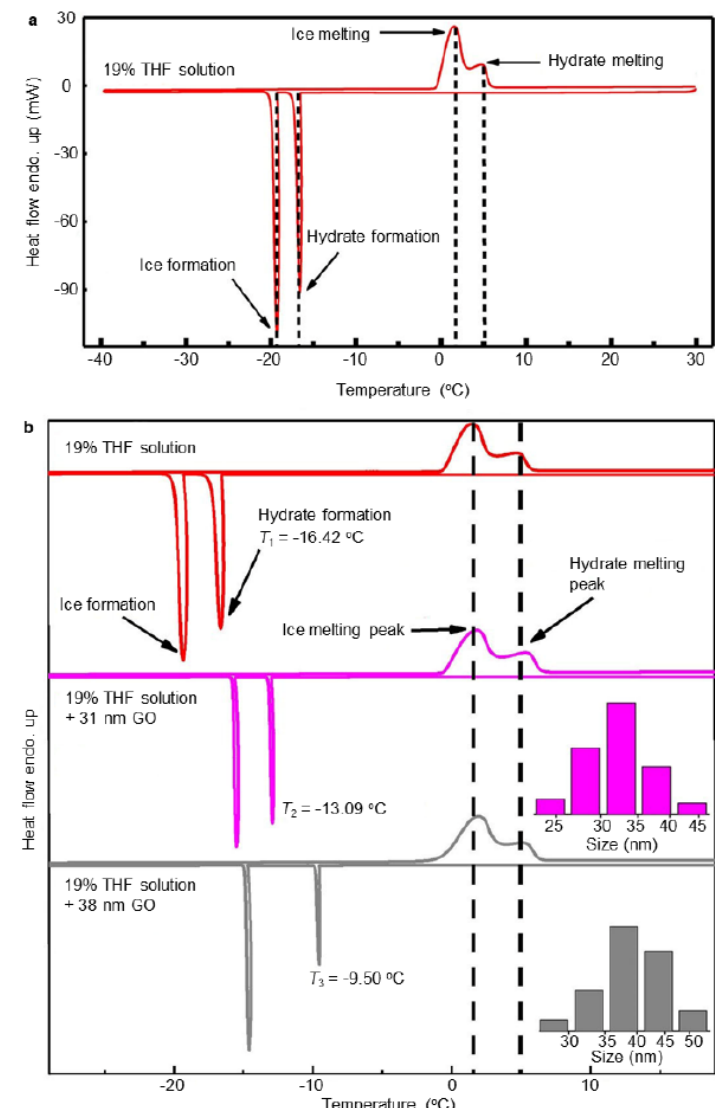
Supplementary Figure 2. DSC scans with two loops and excellent sealing. For showing the elimination of memory effect, we carried out DSC scans of the same sample with two loops shown in (a), in which the sample was kept at 30 °C for 30 minutes after the first-cycle scan (gray line), and then commencing the testing for the second-cycle scan (blue line). The results showed that the THF clathrate hydrate nucleation temperature in the second cycle is not increased. Thus, it indicates that our experimental setup of holding the sample at 30 °C for 30 minutes can eliminate the memory effect in the nucleation tests. Moreover, from (b) and (c), the calculation of formed ice (area of ice peaks) in the two loops are almost the same with the difference of 0.2%, and the formed THF hydrate are also almost the same with the difference of 1.5% (the red and black solid lines in the (b) and (c), respectively), indicating the excellent sealing in DSC scans.



Supplementary Figure 3. Characterizations of GOs of controlled sizes. The GOs (a-3nm, b-8nm, c-13nm, d-22nm, e-46nm, f-78nm) were anchored on the glass surfaces, with AFM imaging and the corresponding height profiles along the white lines marked. (a) - (c), scale bar, 30 nm. (d) - (f), scale bar, 100 nm.



Supplementary Figure 4. Ice formation during cooling the THF solution with various THF/water ratio. **a** The typical DSC thermograph of THF mixed in water with 15 wt% in weight. **b** The melting peak analysis of formed ice and hydrate from (a) solution, respectively. **c** The typical DSC thermograph of THF mixed in water with 19 wt% in weight. **d** The melting peak analysis of formed ice and hydrate from (c) solution, respectively. **e** The typical DSC thermograph of THF mixed in water with 23 wt% in weight. **f** The melting peak analysis of formed ice and hydrate from (e) solution, respectively. **g** The typical DSC thermograph of THF mixed in water with 28 wt% in weight. **h** The melting peak analysis of formed ice and hydrate from (g) solution, respectively. The quantity of ice decreases as increasing the concentration, but reach zero until the concentration is a larger value than the expected 19%, (e.g., 28%), consisting with the argument that the remained water molecules inside the liquid droplet are excessed after the hydrate due to the evaporation of water molecules to the gas space less than the 17 times (the value in the clathrate) of that of THF molecules.



Supplementary Figure 5. Thermal analysis of the formation of THF clathrate hydrates. **a** The typical DSC thermograph of tetrahydrofuran (THF) mixed in water with 19 wt% in weight. The sample was first cooled to -40 °C from 30 °C and then heated to 30 °C. The scan rate in the cooling step is 1 °C min⁻¹ and in the heating step is 5 °C min⁻¹. In the cooling program, the formation of THF hydrate and ice can be distinguished from the two obvious crystallization peaks in the thermal curve, which also corresponding to the double melting peaks in the heating stage. **b** In the cooling program, the formation of THF hydrate and ice can be distinguished from the two obvious crystallization peaks in the thermal curve, which also corresponding to the double melting peaks in the heating procedure. The top red line shows that THF mixed in water with 19 wt%, the hydrate forming around $T_1 = -16.42$ °C. The middle magenta line shows that the hydrate forming around $T_2 = -13.09$ °C with adding GO nanosheets of 31 nm in the THF/water mixture. The bottom gray line shows that the hydrate formation enhanced about $T_3 = -9.50$ °C with adding GOs of 38 nm in the THF/water mixture. The magenta and gray inset corresponding to the size distribution of 31 nm and 38 nm GOs, respectively. Sample volume is 3.0 μ L. The scan rate of cooling curve is 1 °C min⁻¹ and the heating rate is 5 °C min⁻¹.

$$l = \frac{L}{2R_c} \quad (2)$$

$$\Delta T = T_m - \bar{T} \quad (3)$$

$$\Delta T_L = T_m - T_L \quad (4)$$

$$J = \frac{1}{nt_D} \quad (5)$$

$$\tau = nt_D \quad (6)$$

$$J = Ae^{-\Delta G^*/(k_B T)} \quad (7)$$

$$R_c = \frac{2\gamma}{|\Delta\mu|} \quad (8)$$

$$\Delta\mu \approx \Delta S \Delta T \quad (9)$$

$$R_c \approx \frac{2\gamma}{|\Delta S|} \frac{1}{\Delta T} \quad (10)$$

$$\Delta G^*(\Delta T, L) = \Delta G^*(\Delta T, \infty) g(l) \quad (11)$$

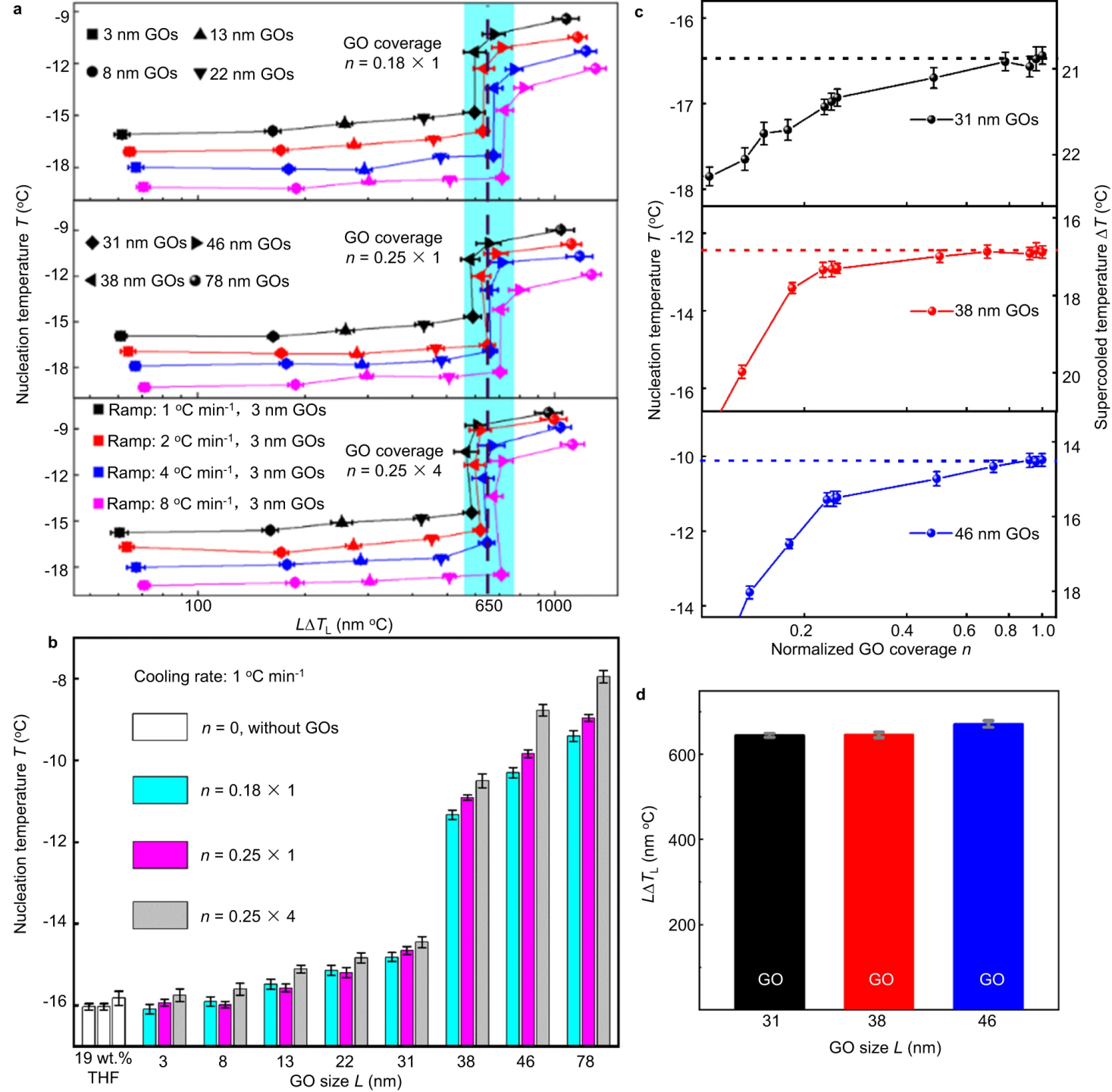


Fig. 2 | Transitions in the THF clathrate hydrate nucleation activity of GO nanosheets at a specific value of the product of GOs' size and the supercooling.

a Relationship between the average nucleation temperature and $L \Delta T_L$ for the THF clathrate hydrate, and the nucleation temperature displays one abrupt change around $L \Delta T_L \approx 650 \text{ nm } ^\circ\text{C}$ for various GO nanosheets with different coverage, $n = 0.18, 0.25$, and 1 , and under different cooling rates (Black-ramp of $1 \text{ } ^\circ\text{C min}^{-1}$, Red-ramp of $2 \text{ } ^\circ\text{C min}^{-1}$, Blue-ramp of $4 \text{ } ^\circ\text{C min}^{-1}$, Magenta-ramp of $8 \text{ } ^\circ\text{C min}^{-1}$). Black – cooling rate $1 \text{ } ^\circ\text{C min}^{-1}$, red – cooling rate $2 \text{ } ^\circ\text{C min}^{-1}$, blue – cooling rate $4 \text{ } ^\circ\text{C min}^{-1}$, and magenta – cooling rate $8 \text{ } ^\circ\text{C min}^{-1}$. Each nucleation temperature was averaged from 100 independent experiments. Error bars are the standard error of the mean (SEM). Data are shown as mean \pm SEM. **b** The average nucleation temperature of THF clathrate tuned by GOs with various average sizes and different coverage of GO nanosheets. The white histograms are the glass substrates without anchored GOs. Cyan – GO coverage of $n = 0.18$, magenta – GO coverage of $n = 0.25$, and gray – GO coverage of $n = 1$. Each nucleation temperature on the substrate without GOs was averaged from 85 independent experiments. Data are mean \pm SEM. Each nucleation temperature on the substrate with GOs was averaged from 100 independent experiments. Data are mean \pm SEM. **c** The THF nucleation temperature raises as increasing the coverage of GOs with the lateral size $L = 31 \text{ nm}$, 38 nm and 46 nm , respectively, but has a size-dependent saturated value T_L (the dashed lines). Black – 31 nm GO, red – 38 nm G, blue – 46 nm GO. Each nucleation temperature was averaged from 100 independent experiments. Data are shown as mean \pm SEM. **d** The product of the saturated supercooling nucleation temperature $\Delta T_L = T_m - T_L$ with the different GO sizes (L) of s is almost a constant, equal to $650 \text{ nm } ^\circ\text{C}$ (the dashed line), for all the GOs with various L . Black – 31 nm GO, red – 38 nm G, blue – 46 nm GO. Each nucleation temperature was averaged from 100 independent experiments. Data are mean \pm SEM.

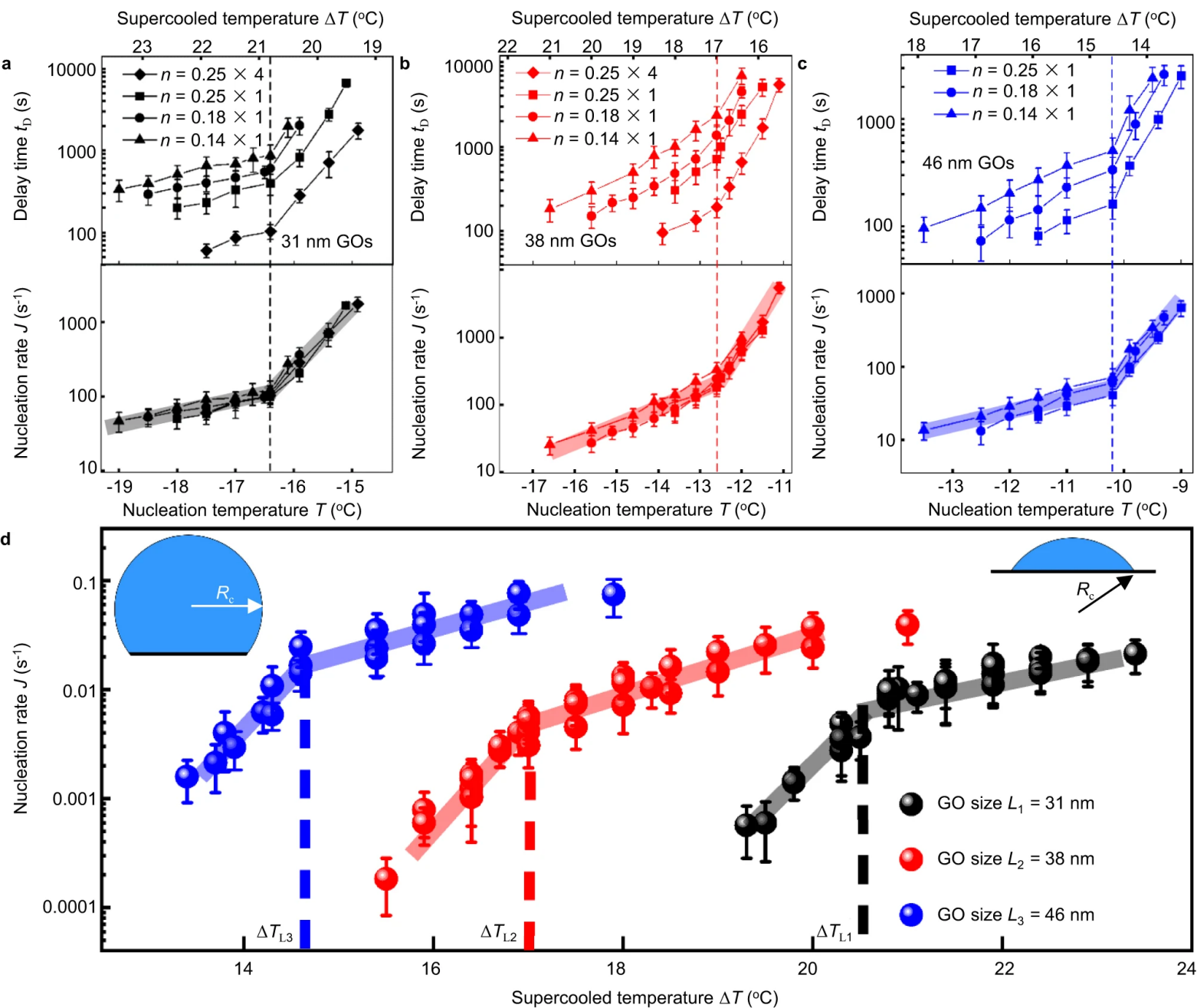


Fig. 3 | Transitions in the nucleation rate during the THF clathrate formation on 31 nm, 38 nm and 46 nm GO nanosheets anchored glass substrates, respectively. a–c The top panels show the (average) delay time t_D of clathrate hydrates of THF-water mixture as the applied constant temperature (and corresponding supercooling shown in top x -axis) for a few n values (the relative number of GO nanosheets as the nucleation sites), and the bottom panels show $\tau = nt_D$ for the same data in the top, as the GO size of 31 nm (black), 38 nm (red), 46 nm (blue), respectively. Abrupt changes (transitions) of the THF clathrate hydrate nucleation activity of GO nanosheets at specific supercooling value depending on the size of applied GO nanosheets. Every average clathrate hydrate nucleation delay time in (a–c) shows mean \pm SEM. For the GO coverage of $n = 0.14$, the mean values were

averaged from 36 measurements. For every other GO coverage ($n = 1$, $n = 0.25$ and $n = 0.18$), the mean values were averaged from 39 measurements. **d** The $J = \frac{1}{\tau}$ gives the nucleation rate of the clathrate on the unit number of GO nanosheets. Black – 31 nm GO, red – 38 nm G, blue – 46 nm GO. The insets show the illustrations of the critical clathrate nucleus on nanosheets as the size of GO nanosheet is smaller (top-left) or larger (top-right) than the spherical diameter of critical clathrate nucleus $2R_c$, respectively, based on the classical nucleation theory. Every average clathrate hydrate nucleation delay time in (d) is processed from (a–c), and shows mean \pm SEM. For the GO coverage of $n = 0.14$, the mean values were averaged from 36 measurements. For every other GO coverage ($n = 1$, $n = 0.25$ and $n = 0.18$), the mean values were averaged from 39 measurements.

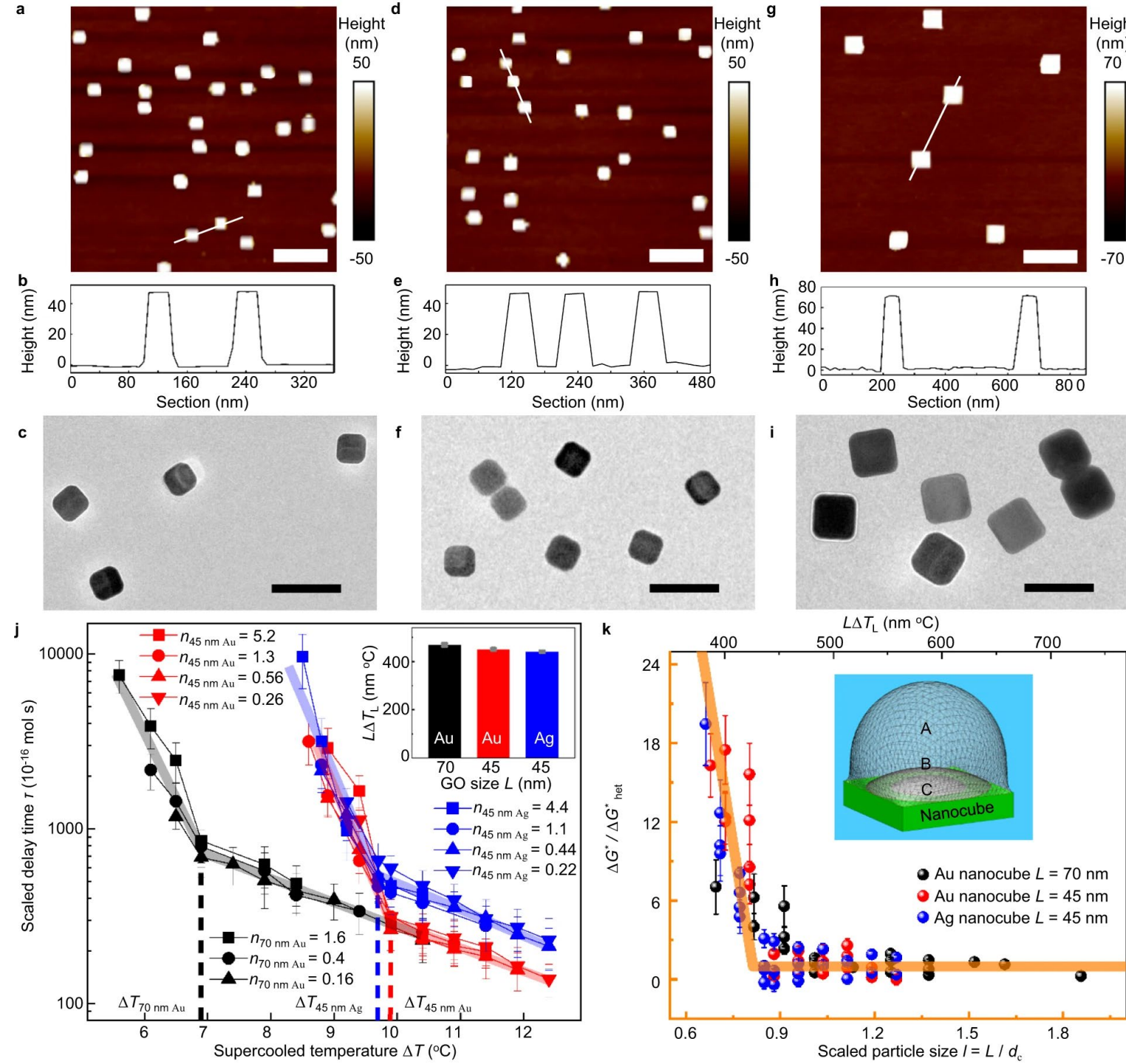


Fig. 4 | Abrupt changes (transitions) of the THF hydrate nucleation activity of Ag/Au nanocubes at specific supercooling temperature ΔT_L which is determined by the size of nanoparticles L . **a–i** The AFM images, corresponding height profiles through the cross-section along the marked lines of anchored nanocubes on the substrate, and TEM images of suspended nanocubes. 45 nm Ag nanocubes (**a–c**), 45 nm Au nanocubes (**d–f**), and 70 nm Au nanocubes (**g–i**), respectively. Scale bar of (**a**), (**d**) and (**g**) AFM images, 200 nm. Scale bar of (**c**), (**f**) and (**i**) TEM images, 100 nm. **j** The scaled delay time of nucleation of THF aqueous solution, $\tau = n\tau_D$, versus ΔT . The three curves for each nanocube come from different n and collapse into the same curve. Black – 70 nm Au nanocube, red – 45 nm Au nanocube, blue – 45 nm Ag nanocube. The inset shows the $L \Delta T_L \approx 450$ nm $^{\circ}\text{C}$ for all the Au and Ag nanocubes. Magenta – 70 nm Au nanocube, cyan – 45 nm Au nanocube, orange – 45 nm Ag nanocube. Every average clathrate hydrate nucleation delay time shows mean \pm SEM. The mean values were averaged from 36 measurements for the 70 nm Au nanocube with coverage of $n = 0.16$, 45 nm Au nanocube with coverage of $n = 0.26$, and Ag nanocube with coverage of $n = 0.22$. For the every other nanocube coverage, the mean values were averaged from 39 measurements. **k** The free-energy barrier of THF hydrate nucleation ΔG^* on the Ag/Au nanocubes in the unit of that on sufficient-large substrates ΔG^*_{het} . The free-energy barrier obtained from the data in Fig. 4j is compared with the theoretical calculation based on the spirit of CNT (orange line and axis, the transition occurs at $l_c = \frac{L}{2R_c} \approx 0.8$ for the nanocubes with the side length L , see Supplementary Fig. 8). Black – 70 nm Au nanocube, red – 45 nm Au nanocube, blue – 45 nm Ag nanocube, orange – fit line and corresponding XY axis. Inset, schematic illustrations of the shapes of clathrate nucleus with various sizes on a nanocube. Every data point in (**k**) is processed from (**j**), and shows mean \pm SEM. The mean values were averaged from 36 measurements for the 70 nm Au nanocube with coverage of $n = 0.16$, 45 nm Au nanocube with coverage of $n = 0.26$, and Ag nanocube with coverage of $n = 0.22$. For the every other nanocube coverage, the mean values were averaged from 39 measurements.

- This experimental study successfully probes the critical nucleus size in THF clathrate hydrates and reveals a crucial relationship between its size and the supercooling level.
- By demonstrating the inverse proportionality of the critical nucleus size to the degree of supercooling, this work contributes valuable insights into the microscopic mechanism of clathrate hydrate nucleation.
- The reported technique of using nanoparticles as the probe is demonstrated to have general feasibility in probing the occurrence and character of the (transient and small) critical nucleus in numerous of the 1st-order phase transition processes.